

Instability study of magnetic journal bearing under supercritical CO₂ cooled MMR conditions

Do Kyu Kim, Seung Joon Baik, Jeong Ik Lee

Department of Nuclear and Quantum Engineering, KAIST, Daejeon, South Korea

Email: mike08@kaist.ac.kr, bsj227@kaist.ac.kr, jeongiklee@kaist.ac.kr

1. Introduction

The newly released International Maritime Organization, IMO regulation forces the diesel engine on the vessels to be replaced to reduce CO₂ emission. Since the ship has limited space, the alternative engine should also be compact. A concept of fully modularized fast reactor with a supercritical CO₂ (S-CO₂) cooled direct Brayton cycle, namely Micro Modular Reactor(MMR), can potentially substitute the diesel engine by meeting those requirements and more. [1]

In case of MMR with 10MWe capacity, the magnetic bearing can be a proper choice for the turbomachinery. This can be readily supported by the previous research, which is also partially shown in Fig 1. MMR's bearing should have larger load capacity than gas foil bearing. In addition, it should be free from oil contamination of CO₂. Therefore, the magnetic bearing is appropriate for the MMR to support the rotor mass with no contamination issues by hermetic condition.

TM Feature	Power (MWe)					
	0,3	1,0	3,0	10	30	100
Bearings	Gas Foil		Hydrodynamic oil			
			Magnetic		Hydrostatic	

Fig 1. Bearing Options for S-CO₂ Brayton Cycles with various power scales [2]

There were several studies related to the bearing for S-CO₂ Brayton cycle application [4 & 5]. However, an instability issue was repeatedly mentioned under high speed operation and S-CO₂ conditions. Shaft orbit under unstable operation is described in Fig. 2. On the other hand, much higher speed operating in air condition does not have this issue (Fig. 3).

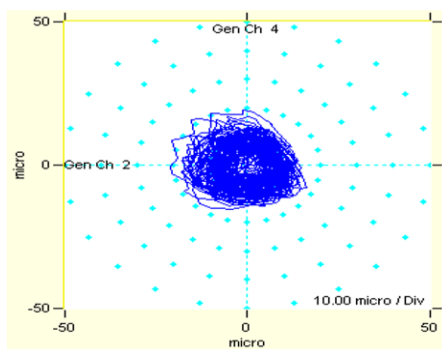


Fig 2. Shaft center orbit at 14,000rpm, 43°C, 78 bar under S-CO₂ condition

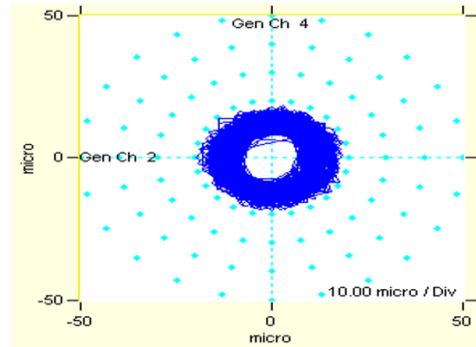


Fig 3. Shaft center orbit at 30,000rpm under air condition

The instability induces the shaft imbalance to grow until the clearance between the shaft and stator disappears leading to crash. As concluded, this instability issue is related to not only the operation speed but also the fluid conditions.

Therefore, the interaction between S-CO₂ lubricating fluid and bearing is modeled with Reynolds equation, which describes the thin film flow. The pressure distribution around the shaft can be calculated from this model. The forces acting on the shaft in S-CO₂ conditions can be compared to the air conditions. In addition, the experimental results can be predicted by the calculation results.

In this paper, the developed S-CO₂ lubrication model is introduced. From the developed model, the magnetic bearing experiment is redesigned based on the calculation results. The experiment focuses on the verification of this model. This verification aims at finding the cause of instability and a method to resolve it. The modified layout of the experiment loop is suggested to achieve the experimental objectives.

2. Methods and Results

2.1 Magnetic journal bearing description

The magnetic journal bearing used in formal experiments has 8 electromagnets to apply the magnetic force to the rotor. The symmetrically located 8 electromagnets as Fig. 4 make possible to consider two axis of rotor separately. The inductive displacement sensor detects the clearance of the bearing so it is used for active control with electromagnets.

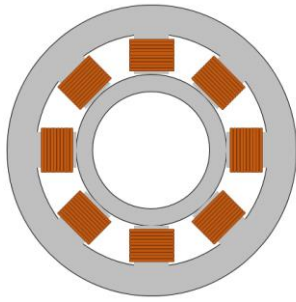


Fig 4. Cross Section of Radial Magnetic Bearing

The empty space in Fig. 4 and 5 is filled with the working fluid. In case of the Brayton cycle, the leaked fluid from the labyrinth seal cools the rotor as well.

Since the spaces between the electromagnets are too complex to formulate for the analysis and potentially a vortex can be generated to destabilize the shaft, the magnetic bearing is planned to have inner-coating to remove the geometry complexity like Fig. 5.

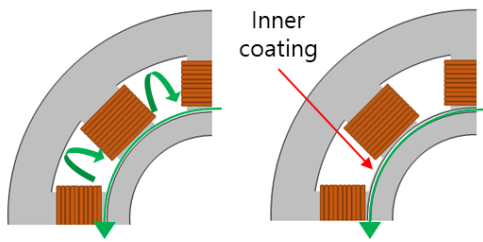


Fig 5. Schematic drawing of the bearing inner coating

2.2 Modeling and experimental scope

The experimental range of the model which will be introduced is described in Table 1. The experimental pressure range is from 1bar to 100bar. This is for the comparison between the high speed operation in air condition and the CO₂ condition with 1bar so the effect of the pressure and the fluid type, density can be compared. The temperature range includes the CO₂'s critical temperature and room temperature. The rotational speed range is from 10000RPM to the 30000RPM. The reason is that the 15000RPM is the highest speed with CO₂ condition near critical point and the 30000RPM is the available speed in air condition. The eccentricity, ϵ is the ratio between the unbalanced length(e) and the averaged gap distance($c = R_2 - R_1$). The geometry is described in Fig. 6.

Table 1. Operation condition range of the model

Supply temperature	10 ~ 50 °C
Supply pressure	1 ~ 100bar
Rotational speed	10000~30000 RPM
Eccentricity, ϵ	0.25~0.75

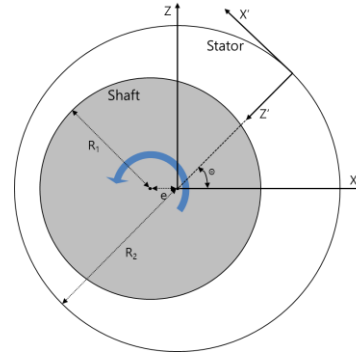


Fig 6. Geometry of the unbalanced shaft and the stator

2.3 Steady turbulent lubrication model of inner coated bearing

Reynolds equation is a partial differential equation for thin film flow. The pressure distribution around the shaft with inner-coated magnetic bearing can be calculated with this equation. It can be derived by substitution of the velocity profile from Navier-Stokes equation into the continuity equation. The equation is

$$\frac{\partial}{\partial X} \left(\frac{\rho h^3}{12\mu} \frac{\partial p}{\partial X} \right) + \frac{\partial}{\partial Y} \left(\frac{\rho h^3}{12\mu} \frac{\partial p}{\partial Y} \right) = \rho \frac{\partial h}{\partial t} + h \frac{\partial \rho}{\partial t} + \frac{1}{2} \frac{\partial(\rho h u)}{\partial X} + \frac{1}{2} \frac{\partial(\rho h v)}{\partial Y} \quad [3]$$

(X : circumferential direction, Y : axial direction, Z : radial direction, t : time, w : radial velocity, u : circumferential velocity, h : gap, ρ : density, μ : viscosity. The X'-Z' frame is denoted as X-Z frame for convenience.)

The axial direction (Y axis) of the equation is assumed to be negligible because the axial velocity is relatively smaller than rotational speed. In addition, the transient term is removed to consider the steady condition only. Therefore, the equation is simplified.

$$\frac{\partial}{\partial X} \left(\frac{\rho h^3}{12\mu} \frac{\partial p}{\partial X} \right) = \frac{1}{2} \frac{\partial(\rho h u)}{\partial X}$$

The turbulence effect can be considered by the new coefficient k_x from the Ng-Pan model, which is $k_x = 12 + K_x (Re)^{n_x}$ instead of the 12 in the left side of the equation ($Re = \rho c u / \mu$). The constants, K_x and n_x in the equation is described in table 2.

Table 2. Coefficient in Ng-Pan model

Reynolds' number	K_x	n_x
50,000 < Re	0.0388	0.8
5000 < Re < 50000	0.0250	0.84
Re < 5000	0.0039	1.06

The equation is numerically solved by finite difference method (FDM). The coordinate and thin film geometry for the FDM is described in Fig. 7.

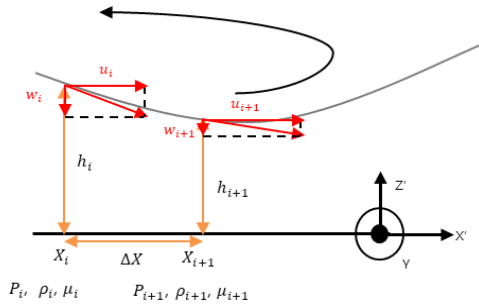


Fig 7. Coordinate description of Reynolds equation

2.4 Analysis of the modeling

Before the experiment, the calculation results from this model should be analyzed. The pressure calculation results are described in Fig. 8.

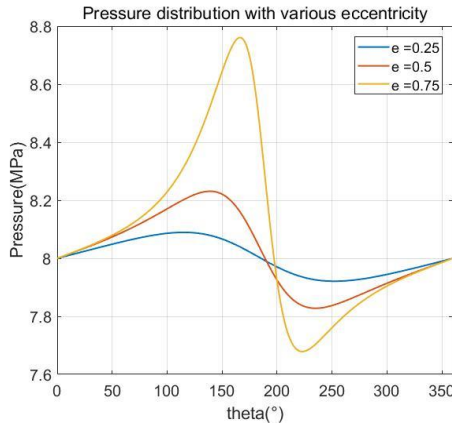


Fig. 8. Pressure distribution around the shaft at 30000RPM, 40 °C and 80bar

From the pressure distribution, the force to the shaft can be calculated. The forces in several conditions are compared and analyzed with Figs below. The horizontal force (F_x) is the force which act in X direction and the vertical force (F_z) is in Z direction from Fig. 6.

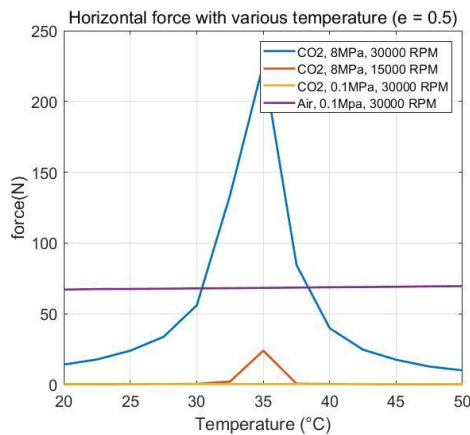


Fig. 9. Horizontal force with various condition, $\epsilon=0.5$

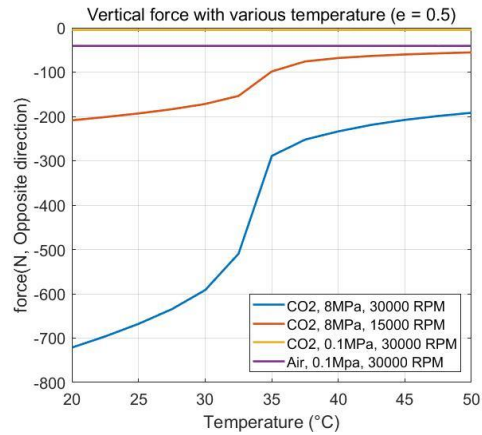


Fig. 10. Vertical force with various condition, $\epsilon=0.5$

From the plot, the F_x in CO₂ condition is sensitive to the temperature especially near the critical point while air condition isn't. Also, F_x in CO₂ condition has maximum values near pseudo-critical point. The F_z in air condition is also insensitive. F_z in CO₂ condition grows as temperature increases.

From this tendency, the sensitive condition especially near the pseudo-critical point is expected to be one of the instability cause. This is described in Fig. 11. In addition, the ratio of the forces of each axis has a different tendency depend on the fluid.

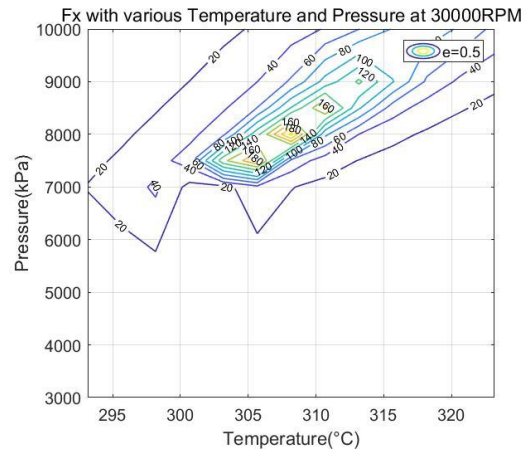


Fig. 11. Horizontal force contour with various thermal condition, 30000RPM, $\epsilon=0.5$

Because of this sensitivity, even though the rotational speed is high, it is concluded that the heat transfer cannot be ignored. The heat transfer analysis is planned to be added.

2.5 Redesigned experimental process

The experimental condition is wide and quite sensitive. Therefore, the CO₂'s thermal state should be controlled. S-CO₂ pressurizing experiment (S-CO₂PE) facility (Fig. 12) will be used for this purpose.

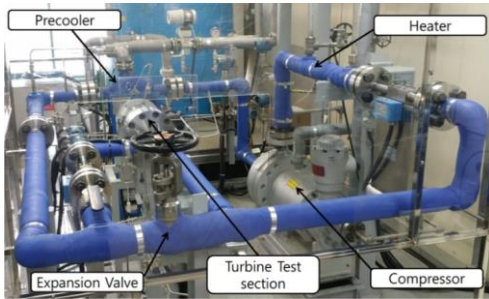


Fig. 12. S-CO₂ power cycle demonstration facility

The magnetic bearing test rig consists of the compressor and the magnetic bearing inside of it. The impeller is removed so only the bearing effect is expected to be dominant. Therefore, the magnetic bearing test rig's discharge port is blocked and the outlet is only the leakage port. It is shown in Fig. 13.

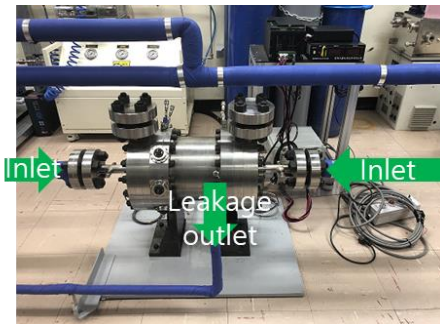


Fig. 13. Magnetic bearing test rig

From this, the S-CO₂PE is upgraded as Fig. 14 & 15. The pressure drop is compensated by the compressor.

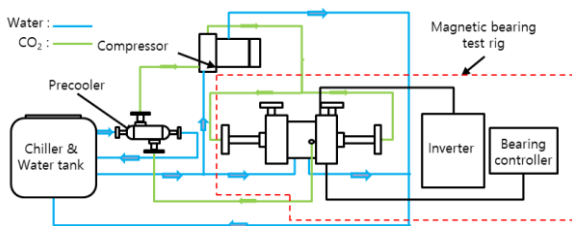


Fig. 14. Layout of the bearing instability experiment

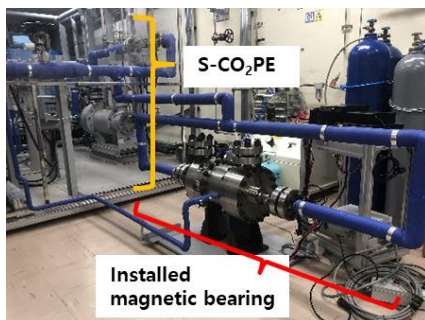


Fig. 15. The magnetic bearing & compressor system for S-CO₂

Firstly, the magnetic bearing test without inner coating is planned under the conditions in Table 1. After this test, the bearing will have inner coating. The second test with inner coated magnetic bearing under the same conditions will be conducted. The second test can be compared to the first test. From this, the geometry complexity effect can be verified.

Those experiment results will be analyzed with shaft center's trajectory. From the trajectory, the net force acted on the shaft can be obtained. Also, the magnetic force can be calculated from the current through the electromagnet. After the rotor dynamic force calculation, we can subtract the force from the fluid. The modeling above can be compared with this results and modified.

3. Conclusions

The developed model is planned to be advanced with heat transfer analysis. This process is also planned to be verified with CFD.

The effect of the unexpected flow will be analyzed from the comparison between the experiments that with and without inner coating. Also, the lubrication modeling will be verified by the trajectory analysis.

From the results, the demanded magnetic bearing performance can be suggested. Also, if the model is well validated, this model can be adapted to various S-CO₂ cycle systems.

Acknowledgement

Authors gratefully acknowledge that this research is funded by Saudi Aramco KAIST CO₂ Management Center.

REFERENCES

- [1] Kim, S. G., Yu, H., Moon, J., Baik, S., Kim, Y., Jeong, Y. H., and Lee, J. I. (2017) A concept design of supercritical CO₂ cooled SMR operating at isolated microgrid region. *Int. J. Energy Res.*, 41: 512–525. doi: 10.1002/er.3633.
- [2] Sienicki, James J., et al. "Scale dependencies of supercritical carbon dioxide Brayton cycle technologies and the optimal size for a next-step supercritical CO₂ cycle demonstration." *SCO₂ power cycle symposium*. 2011.
- [3] Hamrock, Bernard J., Steven R. Schmid, and Bo O. Jacobson. *Fundamentals of fluid film lubrication*. CRC press, 2004.
- [4] Dousti, Saeid, and Paul Allaire. "A compressible hydrodynamic analysis of journal bearings lubricated with supercritical carbon dioxide." *Proceeding of Supercritical CO₂ Power Cycle Symposium, San Antonio, TX*. 2016.
- [5] El-Shafei, A., and A. S. Dimitri. "Controlling journal bearing instability using active magnetic bearings." *Journal of Engineering for Gas Turbines and Power* 132.1 (2010): 012502.